Non-Gaussian statistics and temporal variations of the ultrasound signal backscattered by blood at frequencies between 10 and 58 MHz

Guy Cloutier[a)]
Laboratory of Biorheology and Medical Ultrasonics, Research Center, University of Montreal Hospital and Department of Radiology, University of Montreal, Québec H2W 1R7, Canada

Michel Daronatand David Savéry[b)]
Laboratory of Biorheology and Medical Ultrasonics, Research Center, University of Montreal Hospital, Québec H2W 1R7, Canada

Damien Garcia and Louis-Gilles Durand
Laboratory of Biomedical Engineering, Clinical Research Institute of Montreal, Québec H2W 1R7, Canada

F. Stuart Foster
Department of Medical Biophysics, Sunnybrook and Women's College Health Sciences Centre, University of Toronto, Ontario M4N 3M5, Canada

(Received 21 October 2003; revised 7 April 2004; accepted 22 April 2004)

Very little is known about the blood backscattering behavior and signal statistics following flow stoppage at frequencies higher than 10 MHz. Measurements of the radio frequency (rf) signals backscattered by normal human blood (hematocrit=40%, temperature=37 °C) were performed in a tube flow model at mean frequencies varying between 10 and 58 MHz. The range of increase of the backscattered power during red blood cell (RBC) rouleau formation was close to 15 dB at 10 and 36 MHz, and dropped, for the same blood samples, below 8 dB at 58 MHz. Increasing the frequency from 10 to 58 MHz raised the slope of the power changes at the beginning of the kinetics of aggregation, and could emphasize the non-Gaussian behavior of the rf signals interpreted in terms of the *K* and Nakagami statistical models. At 36 and 58 MHz, significant increases of the kurtosis coefficient, and significant reductions of the Nakagami parameter were noted during the first 30 s of flow stoppage. In conclusion, increasing the transducer frequency reduced the magnitude of the backscattered power changes attributed to the phenomenon of RBC aggregation, but improved the detection of rapid growth in aggregate sizes and non-Gaussian statistical behavior. © *2004 Acoustical Society of America.* [DOI: 10.1121/1.1760791]

PACS numbers: 43.80.n, 43.80.Qf, 43.80.Vj [FD] Pages: 566–577

I. INTRODUCTION

Blood is a heterogeneous suspension of erythrocytes, leukocytes, and platelets in plasma. The scattering of ultrasound by blood is mainly attributed to the erythrocytes, or red blood cells (RBCs), because they are larger and much more numerous than the other blood particles (they constitute around 35%–45% of the blood volume in normal individuals). The phenomenon of RBC aggregation, which is known to have a determinant effect on the ultrasound backscattered signal intensity and spectral slope,[1–3] was described as a blood coagulating and decoagulating event more than 300 years ago.[4] In 1929, Fahraeus studied the sedimentation rate of RBCs in various conditions and depicted aggregation as the binding of erythrocytes to form rouleaux and clusters.[5]

It is known from the contemporary literature that the formation and breakup of aggregates depends on the shearing conditions of the flow, biological factors such as the concentration of certain plasma proteins, and cellular adhesion mechanisms.[6] The rheological impacts of RBC aggregation on blood flow are numerous and affect both the macro- and microcirculation. Among them may be cited its effect on the formation of sludge blood in microvessels,[7] increased blood viscosity,[8] occurrence of vascular thrombosis,[9] increased flow resistance,[10] increased interaction of leukocytes with the endothelium,[11] and hemodynamics.[12] In addition, the ability of blood to perform its main function, i.e., to transport oxygen, carbon dioxide, nutrients, and metabolic products can be affected by RBC aggregation.[13,14]

The main purpose of the present study was to investigate possible changes in the statistics of the ultrasound signal backscattered by blood, at frequencies between 10 and 58 MHz, as a mean to characterize the dynamics of RBC aggregation. Compared to other hemorheological methodologies used in medicine and research, ultrasound penetrates tissues and can provide measurements *in situ*.[15] Mean frequencies between 10 and 58 MHz were selected to cover a wide range of spatial resolutions allowing access to different vessel sizes.

[a)]Director, Laboratory of Biorheology and Medical Ultrasonics, Research Center, Centre hospitalier de l'Université de Montréal, 2099 Alexandre de Sève (room Y-1619), Montréal, Québec, Canada, H2L 2W5. Electronic mail: guy.cloutier@umontreal.ca
[b)]Present address: Philips Research USA, 345 Scarborough Road, Briarcliff Manor, NY 10510, USA.

 0001-4966/2004/116(1)/566/12/$20.00 © 2004 Acoustical Society of America

A. Statistical models and ultrasound tissue characterization

The statistical analysis of the ultrasound radio-frequency (rf) signal and of its envelope (B-mode image) has been used for some years as an approach to differentiate normal and pathological biological tissues. Kuc[16] introduced the coefficient of kurtosis (K_u) as a mean to differentiate Gaussian from non-Gaussian ultrasound signals. The method was applied to characterize the rf signals backscattered by normal livers (Gaussian distribution, $K_u=3$), and by fatty-infiltrated hepatic tissues (uniform distribution, $K_u<3$). It may be noted that a non-Gaussian random variable with a peaking histogram (leptokurtic distribution) results in $K_u>3$. The kurtosis coefficient of a given statistical distribution is defined by the ratio of the fourth central moment to the square of the second central moment of the random variable X

$$K_u=\frac{E[(X-\mu_x)^4]}{E[(X-\mu_x)^2]^2}, \tag{1}$$

where $E[\,]$ represents the ensemble average and $\mu_x=E[X]$.

From here on, let us consider the ultrasound time-domain rf signal as being statistically described by the random variable X. Assuming that the scattering tissue is composed of many independent subscatterers and according to the central limit theorem, the backscattered echo $x(t)$ is Gaussian distributed and the envelope $A(t)$ thus follows a Rayleigh distribution.[17] However, as presented in the present article, the above considerations may not always be valid when $x(t)$ comes from the backscattering of RBCs or RBC aggregates.

To consider the complexity of ultrasound backscattering by biological tissues, and to better characterize the deviation from the Gaussian (for rf signals) and Rayleigh (for B-mode images) distributions, other statistical models were investigated. The K distribution, derived from works in optics, was proposed to study the effect of the concentration of scatterers on the ultrasound speckle statistics of $A(t)$.[18] It was postulated by Weng *et al.*[18] that clustered scattering may result in non-Rayleigh distributions if one considers a small number of scatterers per resolution cell. In their model, the envelope signal $A(t)$ is K distributed, the probability density function (PDF) $P_K(A)$ is being given by

$$P_K(A)=\frac{2b}{\Gamma(M)}\left(\frac{bA}{2}\right)^M J_{M-1}(bA), \tag{2}$$

where the two PDF parameters b and M can be expressed as a function of the moments of the K variable A according to

$$b=\left[\frac{\Gamma(M+1/2)}{\Gamma(M)}\right]\frac{2\Gamma\left(\frac{3}{2}\right)}{\mathrm{E}[A]}$$

and

$$K_u=2\left(1+\frac{1}{M}\right),$$

K_u being the kurtosis of the random variable $A(t)$.
In these equations, Γ is the gamma function, and J_{M-1} is the modified Bessel function of order $M-1$. By considering $A(t)=|x(t)|$, one can derive the following relationship:[19]

$$K_u=3\left(1+\frac{1}{M}\right), \tag{3}$$

where K_u is the kurtosis of the random variable $x(t)$. When M becomes large, the K distribution is equivalent to the Rayleigh distribution, i.e., the envelope signal PDF obtained when $x(t)$ is Gaussian.

Very interestingly, it was shown that the parameter M (effective number density) of the K distribution is physically related to the nonuniformity in scattering cross sections (ν) and to the number of particles in the scattering volume (N), determined by the beam cross section and length of the incident pulse[20]

$$M=N(\nu+1), \quad \nu>-1. \tag{4}$$

It may be worth mentioning that the parameter ν was unfortunately not explicitly defined in the above article. For human blood at a typical hematocrit of 40%, RBC counts are $4.6-6.2\times10^6$ particles per ml for man, and $4.2-5.4\times10^6$ per ml for woman.[1] Thus, because N is very large in a given range cell and because each RBC has a similar acoustic impedance, changes in the number of particles N should play a minor role in affecting the statistics of the backscattered echoes, for the experimental conditions of the present study.

Using simulations, Narayanan *et al.*[21] tested the range of validity of the Rayleigh probability distribution of the B mode signal ($A(t)$). Non-Rayleigh histograms were characterized by the K distribution parameters. As the scattering cross sections became more random ($\nu\rightarrow-1$), the effective number density M was shown to decrease. In the same study, the effect of the scatterer's density (number of scatterers per unit volume) on the departure from the Rayleigh histogram was experimentally verified in a phantom (the K distribution functions were plotted for estimated M values of 0.076, 0.707, and 3.940). *In vivo*, the effective number of scatterers M was used to identify breast tumors,[20] and to study breast and liver tissues.[22,23] Equation (3) of the K distribution model was also considered to characterize *in vitro* non-Gaussian Doppler signals from a suspension of calf RBCs (no aggregation) circulating through a severe stenosis.[24] The clustering of RBCs caused by the acceleration of the flow in the stenotic jet was suggested as a mechanism to explain the non-Gaussian behavior of the backscattered signals ($K_u>3$). A link can thus be made between Eq. (4) and the phenomenon of RBC aggregation, where broad ranges of scatterer's size (parameter ν) may exist depending on the flow conditions.

Other probability distributions were proposed in the field of ultrasound tissue characterization to consider the spatial correlation of complex heterogeneous tissues. These are introduced here because they may complement the information provided by the K distribution. The Rician,[25] homodyned K,[26] gamma,[27] and Nakagami[28] distributions were adapted from the literature in other fields, and used to characterize the envelope of the ultrasound (US) backscattered signal. The Nakagami distribution is relatively simple to characterize and has a PDF given by

$$P_N(A) = \frac{2m^m A^{2m-1}}{\Gamma(m)\Omega^m} e^{-mA^2/\Omega}, \tag{5}$$

where Γ is the gamma function, $\Omega = E[A^2]$ is a scaling factor computed from the envelope $A(t)$, and m, the Nakagami parameter, is given by

$$m = \frac{E[A^2]^2}{E[(A^2 - E[A^2])^2]}. \tag{6}$$

If one considers a large number of scatterers it is, by definition, greater than or equal to $\frac{1}{2}$. As reported in the literature, m is greater than one for a quasiperiodic half-wavelength spacing of particles, whereas for structures showing some level of organization it is between $\frac{1}{2}$ and one.[28] For $m = 1$, the Nakagami distribution is equivalent to the Rayleigh distribution, which corresponds to the case of $x(t)$ being a Gaussian signal scattered by randomly located particles. Because some level of spatial correlation among scatterers may be expected for blood with RBC aggregation,[29,30] the Nakagami parameter m may be of interest to study the backscattered signal by blood.

B. Objectives and hypotheses

In the present study, the first objective was the analysis of the non-Gaussian statistical properties of the backscattered echoes by blood by using the coefficient of kurtosis (K_u) of the rf signal $x(t)$, and the Nakagami parameter (m) of the envelope $A(t)$ obtained by the Hilbert transform of $x(t)$. It was hypothesized that the effective number density of scatterers [parameter M of the K distribution model, Eq. (4)] should decrease during the formation of RBC aggregates because of the presence of disparity in aggregate' sizes within the volume of interest ($\nu \to -1$). This should be reflected by an increase of K_u above 3 during the kinetics of aggregation [Eq. (3)] because of the nonhomogeneity of the scattering crosssections induced by the formation of RBC clusters (for simplicity, RBC aggregates are considered as the basic scattering units for this study). Another hypothesis justifying the use of m [Eq. (6)] is the possibility of identifying regularity in the aggregate structures (if $m > 1$ or $\frac{1}{2} \leqslant m < 1$). A second objective of this study was to extend, to higher frequencies, experimental measurements related to changes in blood echogenicity during the kinetics of RBC aggregation.[31] In the study by Qin *et al.*, horse blood was used and the frequency was limited to 10 MHz.

II. METHODS

A. Description of the flow model

All experiments were performed in the steady flow phantom of Fig. 1. The flow model was composed of a peristaltic pump that circulated human blood from a bottom reservoir to a hermetically closed top reservoir. The height difference between both reservoirs determined the flow rate in the main conduit (measurement chamber). The pressurization of the top reservoir allowed damping of oscillations produced by the pump. A magnetic stirrer was used to continuously mix blood in the top reservoir, thus eliminating the sedimentation of RBCs and contributing to the disaggregation of rouleaux before entering the descending conduit. The entrance length between the top reservoir and measurement chamber was greater than 22 cm (the distance from the on/off valve was 12 cm). A cannulating type flow probe (Carolina Medical Electronics, model EMPCO 300 AP1 1/16) was inserted into the tubing to measure the flow rate in the measurement chamber with an electromagnetic flowmeter (Cliniflow II, model FM701D, King, N.C.). To control the flow rate in the main vessel, two valves were inserted in the model. The one on the left (see Fig. 1) regulated the flow in the measurement chamber, while the right valve on the main conduit was maintained open. This allowed adjustment of the flow (prereduction flow rate) before totally closing the right valve to promote RBC aggregate formation (flow stoppage). Hot water was circulated within the double walls of the bottom and top reservoirs to regulate the temperature of blood at 37 °C.

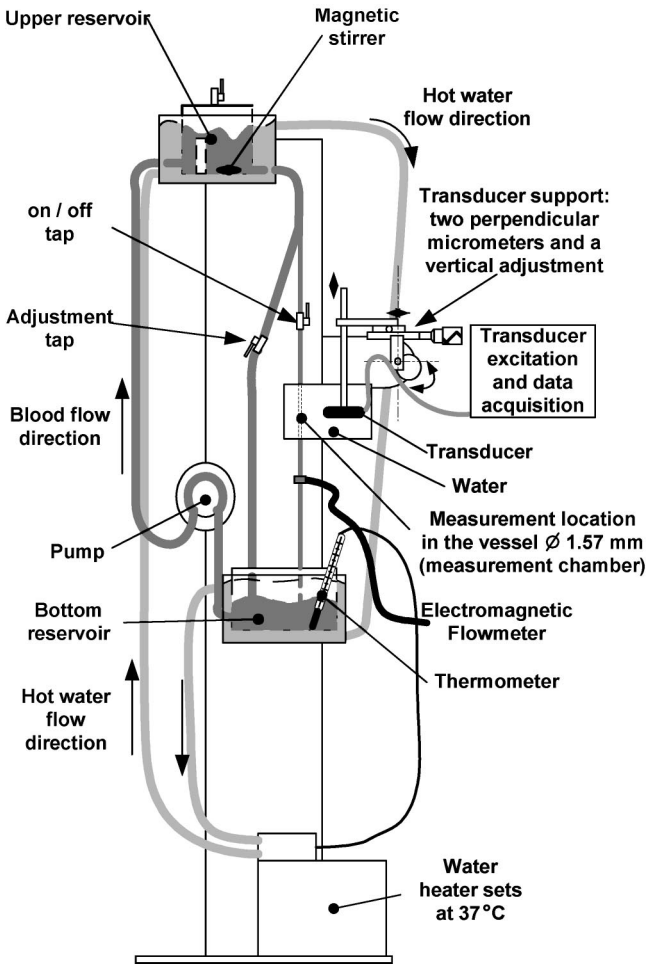

FIG. 1. Schematic representation of the flow loop model used to study the backscattered power and statistics of the ultrasound radio frequency (rf) signals backscattered by blood during the kinetics of red cell aggregate formation.

A closeup view of the measurement chamber is described in Fig. 2. The main wall-less flow conduit, of inner diameter of 1.6 mm, was made by pouring agar gel around a rigid cylinder maintained on both sides by holes made through the walls of an acrylic box. Following the hardening of the gel, the bar was removed to create the lumen. An acoustic window was made in the agar block, in front of the

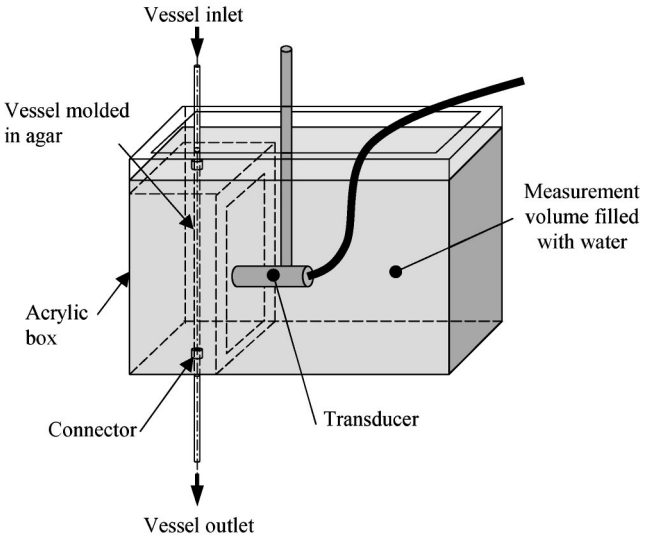

FIG. 2. Closeup schematic description of the measurement chamber.

ultrasound transducer, to adjust the position of the probe. The focused transducer was at 90° with respect to the flow conduit, and the focal point matched the center of the wall-less vessel. The agar gel within an acrylic box and the transducer were immersed in distilled water (room temperature) filling another acrylic container. Connectors allowed the coupling of the measurement chamber with the rest of the flow phantom. The method used to produce the agar gel was described earlier.[32] The gel was made by mixing 3 g of agar powder (Sigma Chemical, high strength agar No. A-6924) with 8 ml of glycerol and 86 ml of distilled water at room temperature. The mixture was then heated at ebullition and progressively cooled to provide hardening. The speed of sound in the solidified gel was close to that of biological tissues (1540 m/s).

B. Blood preparation

Human whole blood and human RBCs, washed and resuspended in saline solution (no aggregation), were used as ultrasound scatterers. The donors were patients suffering from pathologies requiring recurring bleeding of approximately 450 ml. The patients entered into one of these categories: porphyry, hemochromatosis, and polycythemia vera (Vaquez' disease). To our knowledge, these pathologies are not associated to morphological or structural modifications of the RBC membrane, nor to significant changes in the plasma composition. Consequently, it was assumed that the rheology of RBC aggregation was that of normal human blood. Following oral approval by the patient, blood withdrawal was done at the University of Montreal Hospital.

All experiments were done within 24 h of blood collection. For whole blood experiments, the samples anticoagulated with ethylenediamine tetra acetic acid (EDTA) were centrifuged for 20 min at 2300 rpm to separate plasma from blood cells, and the hematocrit was adjusted to 40%. The hematocrit was measured by microcentrifugation at 15 000 rpm for 10 min. For some experiments, the aggregation of RBCs was prevented by using washed erythrocytes. Following the first centrifugation, the plasma was removed and replaced by an isotonic saline solution (Celline II™). After mixing blood, centrifugation was performed again. This procedure was repeated twice to ensure that all plasma proteins responsible for the aggregation were removed. At the end, the washed erythrocytes were mixed with the Celline II solution at a hematocrit of 40%. A volume of approximately 350 ml of blood was necessary to fill the flow model. Before recording any data, the blood sample was introduced in the phantom, and circulated for approximately 1/2 h to eliminate air bubbles and to raise blood temperature to 37 °C.

For each experiment, a blood sample of 1.5 ml was taken from the flow model to measure the aggregation. The erythrocyte aggregation level was determined with a validated erythroaggregameter (Regulest, France) based on a Couette flow configuration.[33] The instrument provides measurements on the aggregation kinetics following flow stoppage, and on the shear rates necessary to partially or totally break RBC rouleaux. A list of aggregation indices measured with this instrument is provided in Sec. III. Blood viscosity measurements were also performed with a cone–plate rheometer (Brookfield, MA, model LVDVIII-CP-42, cone angle$=1.56°$). One ml of blood was withdrawn from the flow model and sheared from 288 to $1\,s^{-1}$ in the rheometer. At each step shear rate, 30 s were allowed to obtain a steady state of viscosity. Measurements were discarded if the torque of the instrument, at a given shear rate, was not high enough to produce repeatable results.

C. Hemodynamic conditions

An analytical biomechanical model was used to determine the velocity profile and thus the shear rate condition before stopping the flow in the phantom. This was required because no measurement of velocity profiles could be performed in the small vessel considered (diameter$=1.6$ mm). For the case of a laminar non-Newtonian steady flow in a rectilinear tube, the velocity profile $V(r)$ of an incompressible fluid can be defined by the following equation:[34]

$$\mu \frac{\partial V}{\partial r} = \frac{1}{2} r \frac{\partial P}{\partial z}, \tag{7}$$

where μ is the dynamic viscosity of the fluid, r is the radial position within the tube, z is the longitudinal distance along the tube, and $\partial P/\partial z$ is the pressure gradient. Since blood is a non-Newtonian fluid, its viscosity μ varies as a function of the shear rate $\partial V/\partial r$. For $\mu = f(\partial V/\partial r)$, one can note that the above equation only depends on $V(r)$. As mentioned earlier, the dynamic viscosity μ was measured for each blood sample by using a cone–plate viscometer.

Knowing the relation $\mu = f(\partial V/\partial r)$ from experimental measurements and the prereduction flow rate that was set to 40 ml/min for all experiments, the numerical solving of Eq. (7) is straightforward. For a given pressure gradient $\partial P/\partial z$, there is only one solution $V(r)$ that corresponds to the limit conditions of the problem. A dichotomic iterative method was used to solve Eq. (7). For a fixed value of $\partial P/\partial z$, $V(r)$ and the related flow rate were calculated. If the flow rate did not match the experimental value of 40 ml/min, $\partial P/\partial z$ was

changed and $V(r)$ was recalculated. When the solution was found, the mean and maximal shear rates were estimated as follows:

$$\overline{\gamma} = \frac{2}{R^2}\int_0^R \frac{\partial V}{\partial r} r \; dr$$

and

$$\gamma_{\max} = \left.\frac{\partial V}{\partial r}\right|_{r=R}, \tag{8}$$

where R is the radius of the tube.

D. Ultrasound transducers

The ultrasound signals were collected with three focused transducers with mean frequencies at 10, 36, and 58 MHz. The descriptions given below were provided by the manufacturers. For all transducers, the frequency response was measured in water, at room temperature, by using a flat reflector positioned at 90° with respect to the probe. The pencil-type piezoelectric (PZT) narrow-band 10 MHz transducer had a diameter of 3 mm, a focal length at 15 mm, and a bandwidth at −6 dB ranging from 7.6 to 12.4 MHz (Etalon Inc., Lebanon, IN). Two wideband polyvinylidene flouride (PVDF) transducers were used to collect data at higher frequencies (Visualsonics, Toronto, Canada). The 36 MHz transducer had a diameter of 3 mm, a focal length at 6 mm, and a bandwidth ranging from 18 to 54 MHz at −6 dB. The probe at 58 MHz had a diameter of 2 mm, a focal length at 4 mm, and a bandwidth of 30–77 MHz (−6 dB).

E. Data acquisition

Two different pulser–receiver instruments were used to collect the rf ultrasound data at a pulse-repetition frequency (PRF) of 1 kHz. A Panametrics system (model 5900 PR, Waltham, MA) was used to transmit negative impulses to the 10 MHz transducer. The echoes backscattered by blood within the vessel lumen were amplified and filtered between 1 and 20 MHz by the Panametrics receiver. An ultrasound biomicroscope (Visualsonics, model UBM VS40) was used to pulse the high-frequency transducers with bipolar square waves (the frequencies available were 19, 25, 40, or 55 MHz). The biomicroscope was operated in rf mode. To facilitate the experiments, the probe was not fixed to the moving scan head during recordings of data. The 36 MHz transducer was fired at 19 MHz and a bandpass filtering between 5 and 40 MHz was applied to the received echoes. The excitation frequency was 55 MHz and the bandpass filter covered the range of 30–80 MHz for the 58 MHz transducer. For experiments performed with the ultrasound biomicroscope, the excitation frequencies and bandpass filtering values were selected to reduce overlap in the frequency response of the backscattered ultrasound signals.

The PRF trigger at 1 kHz of the Panametrics and Visualsonics systems were used to synchronize the acquisition of the backscattered echoes by an 8-bit Gagescope acquisition board (model 8500 CS, Montreal, Canada). The rf signal was digitized at 500 MHz by using the following multiple record acquisition strategy. Ten successive echoes from within the vessel lumen were acquired and stored into the memory of the Gagescope (typically 750 samples or 1.5 μs of data were acquired from a window centered with the tube axis for each excitation pulse separated by a duration of 1 ms). A delay of 3 s was allowed between each record of ten echoes to transfer the data to a microcomputer. This process was repeated for a duration of 1 min before stopping the flow, and for more than 6 min during the process of RBC aggregate formation. For each blood sample studied, measurements were performed with the three transducers. The selection order of the probe frequency was randomly chosen to avoid time effect in the interpretation of the results. For a given blood sample and probe frequency, measurements were repeated five times for averaging purposes. A total of six experiments with different blood samples were performed (three whole blood and three saline suspended RBC experiments).

F. Kurtosis and Nakagami estimates and confidence intervals

Having obtained a finite number N_s of random samples $[X_1,\ldots,X_{Ns}]$ that satisfies the same PDF [computed from the rf signal $x(t)$ or envelope $A(t)$], one wants to assess the kurtosis and Nakagami parameters of the underlying distribution of X. The empirical mean

$$M_1 = \frac{1}{N_s}\sum_{i=1}^{N_s} X_i, \tag{9}$$

and the central empirical moments

$$M_k = \frac{1}{N_s}\sum_{i=1}^{N_s} (X_i - M_1)^k \tag{10}$$

are first defined. They are biased estimators of the kth central moments of X for $k>1$. The two random quantities $\hat{K}_u$ and $\hat{m}$ given by the equations

$$\hat{K}_u = \frac{M_4}{M_2^2} \tag{11}$$

and

$$\hat{m} = \frac{(M_2 + M_1^2)^2}{\frac{1}{N_s}\sum_{i=1}^{N_s} (X_i^2 - M_2 - M_1^2)^2}, \tag{12}$$

are then estimators of the kurtosis and Nakagami parameters that are used from now. Considering that $\hat{K}_u$ and $\hat{m}$ can take random values around the real K_u and m, a convenient method must be used to interpret them and to assess their robustness.

The estimator $\hat{K}_u$ was used to test if the random signal X was effectively Gaussian. Let $H0$ be the hypothesis "X is a Gaussian variable." Under $H0$, $\hat{K}_u$ has a certain PDF, which is independent of the mean and standard deviation of X but dependent on N_s. Using many Monte Carlo simulations of unit centered normal variables (in our case, 10 000 simulations of N_s Gaussian variables), the histogram of $\hat{K}_u$ and the

TABLE I. RBC aggregation indices measured with the erythroaggregameter at 37 °C. The hematocrit was 40% for all measurements.

RBC[a] aggregation indices	Washed human RBCs[a] ($n=3$)	Calf blood[f] ($n=10$)	Human blood ($n=3$)	Normal human blood[f] ($n=19$)
tA (s)[b]	318 ± 108	N/A[g]	3.3 ± 0.5	2.9 ± 0.8
S_{10} (no unit)[c]	10.70 ± 0.04	N/A[g]	19 ± 2	23 ± 3
γD (s^{-1})[d]	18 ± 3	23 ± 13	40 ± 16	49 ± 4
γS (s^{-1})[e]	20 ± 6	27 ± 16	102 ± 39	119 ± 18

[a]Red blood cell.
[b]Aggregation time.
[c]Aggregation index at 10 s.
[d]Partial dissociation shear rate.
[e]Total dissociation shear rate.
[f]Data reproduced from Ref. 35.
[g]Not available.

95% confidence interval $G_1(N_s)$ for the value $|\hat{K}_u-3|$ (the absolute error of estimation) were computed under the hypothesis $H0$:

$$P(|\hat{K}_u-3|\leqslant G_1(N_s)|H0)=0.95. \tag{13}$$

Using measured data, if the estimated kurtosis $\hat{K}_u$ did not fall inside the interval $[3-G_1(N_s);\ 3+G_1(N_s)]$, then the hypothesis $H0$ of normality of the random samples was rejected.

A similar approach was used to test if a given random positive signal envelope satisfied the Rayleigh distribution by using the Nakagami parameter that is theoretically one in this case. The N_s dependent PDF of $\hat{m}$ was estimated by using many simulations of Rayleigh variables and the hypothesis $H1$: "X is a Rayleigh random signal" was considered. One can then extract a value for $G_2(N_s)$, the 95% confidence interval of the error of estimation $|\hat{m}-1|$

$$P(|\hat{m}-1|\leqslant G_2(N_s)|H1)=0.95. \tag{14}$$

In the case that $\hat{m}$ differed from 1 by more than $G_2(N_s)$, then the hypothesis $H1$ was rejected.

III. RESULTS

A. Aggregation levels

Table I summarizes the aggregation indices measured with the erythroaggregameter. The third and last columns show results reported in the literature for calf blood (no aggregation), and normal human blood collected from young healthy volunteers.[35] It is well known that bovine blood does not form RBC aggregates. The instrument provided measurements of aggregation indices following flow stoppage (tA in seconds and S_{10} no unit), and shear rate values necessary to break rouleaux (γD and γS in s^{-1}). The parameter tA is the aggregation time, S_{10} is the aggregation index at 10 s, and γD and γS are the partial and total dissociation shear rates, respectively. A complete description of those indices can be found elsewhere.[36] The aggregation kinetics is inversely proportional to tA. In other words, a low value of tA indicates rapid formation of RBC aggregates. On the other hand, low values of S_{10} indicate a slow kinetics, and small γD and γS signify fragile aggregates. As observed in Table I, very little, if any aggregation, was found for the washed human erythrocytes (γD and γS are similar to values measured for calf blood). For the human blood samples, the parameters were close to the data reported earlier by our group for healthy subjects.[35] This indicates that the levels of aggregation measured for the patients with porphyry, hemochromatosis, and polycythemia vera were similar to those of normal human blood.

B. Hemodynamic conditions

As discussed earlier, the solution of Eq. (7) for $V(r)$ provided an estimate of the hemodynamic flow conditions before closing the valve to promote the formation of RBC aggregates. The dynamic viscosities μ, measured for each experiment, were used in this equation. The non-Newtonian property of blood did not affect the velocity profiles for the conditions of the present study. For instance, the estimates of $V(r)$ were very similar for whole blood ($n=3$) and RBC suspension ($n=3$) experiments. The velocity profiles ($n=6$) were parabolic with mean velocities of 34.4 ± 0 cm/s [mean $\pm$ standard deviation, the standard deviation is zero because the mean velocity is computed from the prereduction flow rate that is imposed in the model of Eq. (7)], maximum centerline velocities of 68.6 ± 0.2 cm/s, mean shear rates of $1170\pm0\ s^{-1}$, maximum shear rates at the wall of $1755\pm6\ s^{-1}$, and Reynolds numbers of 182 ± 13 (laminar flow). For the entrance length considered in Fig. 1 (>12 cm), fully developed parabolic flow profiles were expected since the non-Newtonian effects are nonsignificant. According to these shear rate values, it is reasonable to postulate that all RBC aggregates were disrupted before stopping the flow.

C. Power and frequency content of the backscattered signals

Figure 3 presents the rf backscattered power variations following flow stoppage for both RBC suspension and whole blood experiments. The backscattered power was computed from the time domain signal by summing the squared values of the rf signal $x(t)$ over the time window considered (10 ms, ten records of 1.5 μs separated by time intervals of 1 ms). The results are shown for transducer mean frequencies of 10, 36, and 58 MHz. For all measurements, the backscattered power before stopping the flow (at $t=0$) was averaged

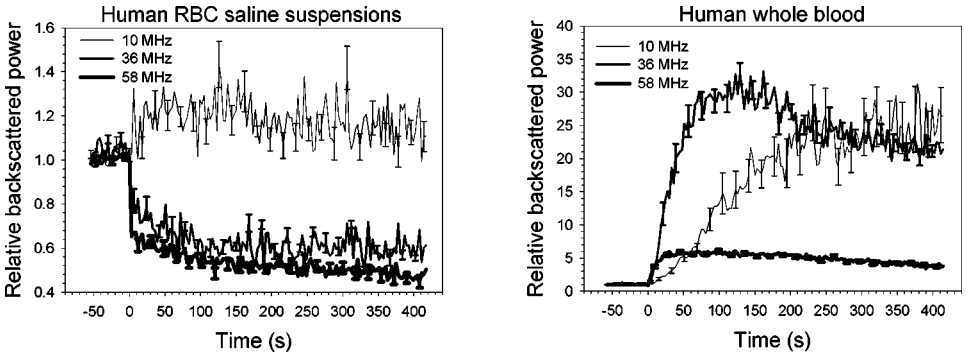

FIG. 3. Relative changes in the ultrasound backscattered power for human RBCs suspended in saline and human whole blood at a hematocrit of 40%, and a temperature of 37 °C. The measurements were performed with three transducers at mean frequencies of 10, 36, and 58 MHz. The standard errors are only displayed for selected times to reduce the density of the graphs ($n=15$; three blood samples and five measurements per sample).

and set to one to facilitate comparisons. For RBC suspensions, a slight increase of the backscattered power (below 1 dB) was observed at 10 MHz following flow stoppage. At 36 and 58 MHz, the power dropped rapidly after flow stoppage by factors of approximately 1.7 times (-2.2 dB) and 2.2 times (-3.5 dB), respectively, after more than 6 min of flow stoppage. For human whole blood, much larger changes in backscattered power were observed during the kinetics of RBC aggregate formation. At 10 MHz, the power increased 26-fold (14.2 dB) between 0 and 410 s. At 36 MHz, the rate of increase of the backscattered power, between 0 and 70 s, was much faster than at 10 MHz. The maximum reached after 70 s corresponded to changes in backscattered power of more than 15 dB (32 times). A reduction of the power by approximately 2 dB was noted following the maximum. The rate of increase of the power was similar between measurements at 36 and 58 MHz, for the first few seconds following $t=0$. However, at 58 MHz, the plateau was reached earlier and the power increase was below 8 dB (6.3 times).

To allow comparisons of the frequency bandwidths measured in water with the three transducers (as provided by the manufacturers) to those obtained from the flow model, the power spectra of the rf backscattered signals at the end of the kinetics of aggregation were computed. For each transducer, an average spectrum was evaluated from the spectra of 1500 rf lines (10 rf lines$\times$10 records separated by 3 s between 384 and 414 s$\times$5 measurements per sample$\times$3 blood samples). Figure 4 combines the results for the three transducers. The mean frequencies within -20 dB of the main lobe were, respectively, 11, 22, and 42 MHz, which is similar to or lower than the mean values of 10, 36, and 58 MHz measured in water with a flat reflector. The frequency chosen for the transmitted pulses, the bandpass filters selected, the frequency-dependent attenuation of blood, and artifacts produced by the measurement chamber can explain the differences. For RBCs suspended in saline, the mean frequencies were 11, 23, and 47 MHz, respectively (results not shown). The lower frequency-dependent attenuation in the absence of RBC aggregation can explain the higher mean frequencies obtained for RBC suspensions with the two highest frequency transducers. From here on, to avoid ambiguity, the transducers are still designated as the 10, 36, and 58 MHz probes.

D. Coefficient of kurtosis

Figure 5 describes the coefficients of kurtosis as a function of time for both RBC suspension and whole blood experiments at 10, 36, and 58 MHz. Similar results were obtained for both types of blood. To this matter, the formation of RBC aggregates following flow stoppage did not affect significantly the estimates of the coefficients of kurtosis. At 10 and 36 MHz, Gaussian rf signals with $\hat{K}_u$ close to 3.0 were observed for both types of blood (most values were within the confidence interval). Increasing the transducer frequency to 58 MHz raised the values of $\hat{K}_u$ slightly above the Gaussian limit.

Since it was hypothesized that disparity in scatterer sizes within the volume of interest may produce non-Gaussian scattered signals, the coefficients of kurtosis were recomputed by considering four window durations for which different ranges of aggregate sizes would be expected. The same strategy was also applied for the suspensions of RBCs but as expected, changing the window length had no effect on the values of $\hat{K}_u$ (the results are not shown but they were similar to those of Fig. 5—left panel). Window durations of 12, 30, 42, and 60 s were considered. Increasing the window length systematically emphasized the non-Gaussian behavior of the backscattered signals for human whole blood, whatever the frequency ($\hat{K}_u$ progressively increased for larger windows). From here on, only the results for a window du-

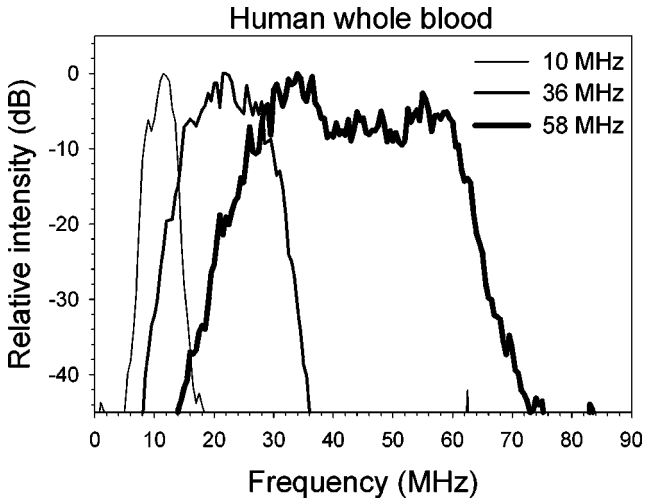

FIG. 4. Normalized power density spectra of the rf signals backscattered by human whole blood at a hematocrit of 40%, and a temperature of 37 °C. The maximum of each mean spectrum was normalized to 0 dB. The measurements were obtained from the flow phantom of Fig. 1, by using three different transducers. The 10 MHz transducer was fired by negative impulses, whereas the 36 and 58 MHz probes were excited by bipolar square pulses at 19 and 55 MHz, respectively.

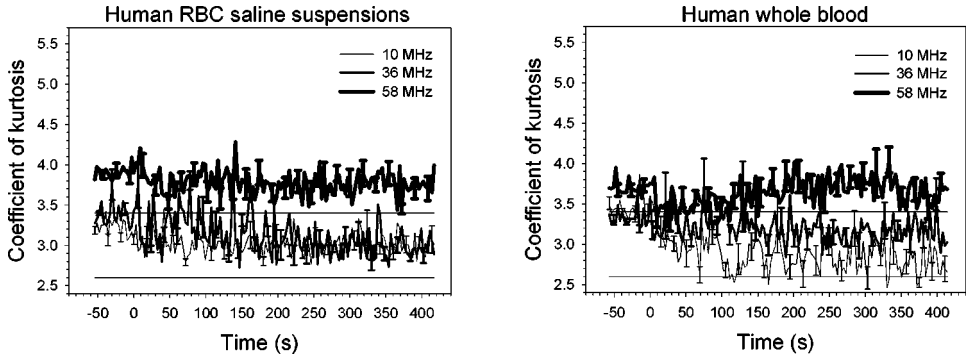

FIG. 5. Coefficient of kurtosis ($\hat{K}_u$) for human RBCs suspended in saline and human whole blood at a hematocrit of 40%, and a temperature of 37 °C. A time window of 10 ms was considered for the computation of $\hat{K}_u$. The measurements were performed with three transducers at mean frequencies of 10, 36, and 58 MHz. The standard errors are only displayed for selected times to reduce the density of the graphs ($n=15$; three blood samples and five measurements per sample). The horizontal lines correspond to the confidence interval of the estimates $[3\pm G_1(N_s)$, as defined by Eq. (13)].

ration of 42 s are presented. At 10 MHz, as shown in Fig. 6, a significant increase of $\hat{K}_u$ to 3.8 was observed during the first few seconds following flow stoppage. Between 120 and 420 s, $\hat{K}_u$ values were close to the confidence interval. The non-Gaussian effect was largely amplified at higher frequencies. Maximum averaged values of $\hat{K}_u$ close to 5.4 were obtained at 36 and 58 MHz. For the three frequencies considered, the peaks of $\hat{K}_u$ occurred between 18 and 27 s after flow stoppage.

E. Coefficient of Nakagami

According to Fig. 7, the information conveyed by the coefficient of Nakagami seems to be very similar to that provided by the coefficient of kurtosis. For instance, each panel of Fig. 7, obtained from the instantaneous rf signal envelopes, is close to a mirror of that presented in Fig. 5. At a given time instant and frequency, an increase of $\hat{K}_u$ corresponds to a similar reduction of $\hat{m}$, and vice versa. As reviewed in Sec. I, a Gaussian rf signal gives $m=1$. For the human erythrocytes suspended in saline, the rf signals were Gaussian at 10 and 36 MHz. At 58 MHz, the same blood samples resulted in non-Gaussian backscattered signals with $\hat{m}$ close to 0.7. For whole blood, the rf signals were generally Gaussian except for some results at 10 and 58 MHz. Surprisingly, non-Gaussian behavior was found at 10 MHz after approximately 100 s of flow stoppage. Figure 8 summarizes, for human whole blood, the results of the coefficients of Nakagami for a window of 42 s. Increasing the window length emphasized the non-Gaussian property of the rf signals, especially at 36 and 58 MHz. The increase in the size of aggregates during the first few seconds of rouleau formation clearly reduced the values of $\hat{m}$. The minimums reached after 10–25 s following flow stoppage were below 0.4. As reported before for the coefficient of kurtosis, using a window of 42 s (or any others between 12 and 60 s) had very little effect on $\hat{m}$ for the RBC suspension experiments (the results are not shown but they were similar to those of Fig. 7—left panel).

IV. DISCUSSION

A. Ultrasound backscattered power variations

The following discussion intends to provide an explanation for the results of Fig. 3 (left panel). It is known that flow disturbance can increase the echogenicity of RBC suspensions,[37,38] if the number density of scatterers is sufficient to provide variance in their spatial distribution (that variance affects the packing or structure factor). Changes in echogenicity on the order of 3–5 dB were reported at frequencies of 10 MHz and below, for hematocrits higher than 10%, approximately. It is not clear, in Fig. 3 (left panel), why stopping the flow provided a slight increase on the order of 1 dB of the backscattered power at 10 MHz. This increase may not be significant, considering the standard deviations reported. A more robust explanation can be provided for the results at 36 and 58 MHz. As seen on the left panel of Fig. 3, the backscattered power was higher by approximately 2.2 and 3.5 dB at 36 and 58 MHz, respectively, before stopping

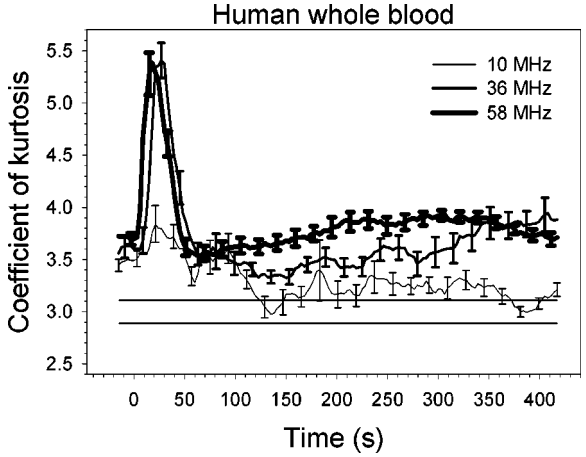

FIG. 6. Coefficient of kurtosis ($\hat{K}_u$) for human whole blood at a hematocrit of 40%, and a temperature of 37 °C. A time window of 42 s was considered for the computation of $\hat{K}_u$. The measurements were performed with three transducers at mean frequencies of 10, 36, and 58 MHz. The standard errors are only displayed for selected times to reduce the density of the graphs ($n=15$; three blood samples and five measurements per sample). The horizontal lines correspond to the confidence interval of the estimates $[3\pm G_1(N_s)$, as defined by Eq. (13)].

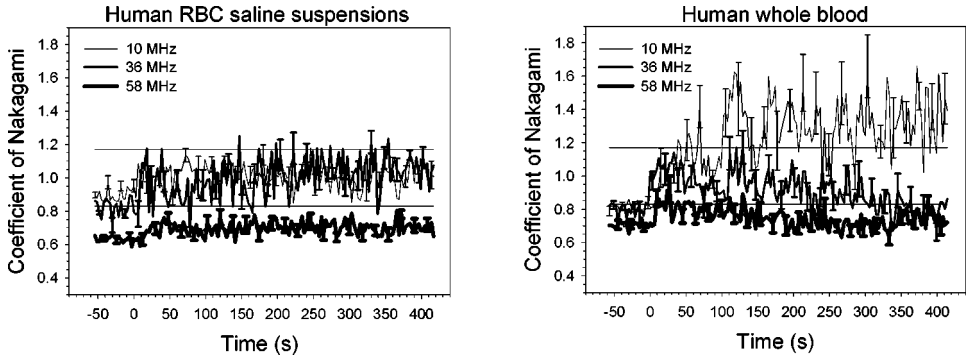

FIG. 7. Coefficient of Nakagami ($\hat{m}$) for human RBCs suspended in saline and human whole blood at a hematocrit of 40%, and a temperature of 37 °C. A time window of 10 ms was considered for the computation of $\hat{m}$. The measurements were performed with three transducers at mean frequencies of 10, 36, and 58 MHz. The standard errors are only displayed for selected times to reduce the density of the graphs ($n=15$; three blood samples and five measurements per sample). The horizontal lines correspond to the confidence interval of the estimates $[1\pm G_2(N_s)$, as defined by Eq. (14)].

the flow. This seems to indicate that a Reynolds number, as low as 182 before flow stoppage, may be sufficient to provide variance in the RBC spatial distribution that is detectable at high frequencies. This suggest that the use of transducers at 36 and 58 MHz may improve the detection of blood flow disturbances with ultrasound, but this still needs to be confirmed. Very interestingly, Lookwood *et al.*[39] reported an increase by 1.6 times of the backscattering coefficient at a mean frequency close to 50 MHz when the flow in a phantom was increased from 18 to 36 cm/s. Flow turbulence was then postulated as a possible mechanism to explain the backscattered power increase (RBC aggregation was prevented in these experiments).

Very little is known about the backscattering of ultrasound by whole blood at high frequencies.[3,40] To our knowledge, the kinetics of RBC aggregation following flow stoppage has never been studied at frequencies higher than 10 MHz.[31,41,42] According to Fig. 3 (right panel), increasing the ultrasound frequency seemed to improve the sensitivity of the method to rapid changes in RBC aggregate sizes by decreasing the time response of the US power. On the other hand, it can be observed in Fig. 3 that the range of variation of the backscattered power during the kinetics of aggregation was much lower at 58 MHz (8 dB) then at 36 MHz (15 dB) or 10 MHz (14.2 dB). Although only one human blood sample was analyzed in their study, Foster *et al.*[3] also noticed a lower sensitivity to the phenomenon of RBC aggregation at high frequency. For instance, by studying the backscattering coefficient as a function of the shear rate and frequency they observed, at 35 MHz, a 14.3 dB variation between 0.1 and 100 s^{-1}, and a variation of only 2.9 dB, for the same range of shear rate, at 70 MHz. Very recent simulation results[29,43] predicted the reduced sensitivity of US backscattering to the phenomenon of RBC aggregation at high frequency. The reduction of the sensitivity was attributed to a decrease of the spectral slope at frequencies above 30 MHz, approximately (the fourth power frequency dependence of US backscattering, which is characteristic of Rayleigh scatterers, is no longer valid in the presence of RBC aggregation at these frequencies; consequently, for a step increase in aggregate sizes, smaller power enhancements are obtained at high frequencies).

According to the results of Fig. 3 (right panel), increasing the frequency from 10 to 36 MHz seemed to be beneficial for the application in hand because the rate of increase of the backscattered power for small changes in aggregate sizes (at the beginning of the kinetics of aggregation) was raised, without significant reduction in sensitivity to large variations in aggregate dimensions during the whole process of RBC rouleau formation. This result is interesting and may deserve more attention. For instance, it would be of interest to determine which frequency between 10 and 36 MHz is optimal to detect dynamic changes in RBC aggregate sizes. The observations of Fig. 3 also may be of interest to interpret the cyclic variations in echogenicity observed at various frequencies under pulsatile flow.[44,45] Finally, this study had a limitation that may deserve discussion. Because three different transducers with different aperture sizes, focal distances, and frequencies were used, the scattering volumes were different. To allow comparison of the results, the mean backscattered power before flow stoppage had to be normalized to one for each transducer, and only relative backscattered

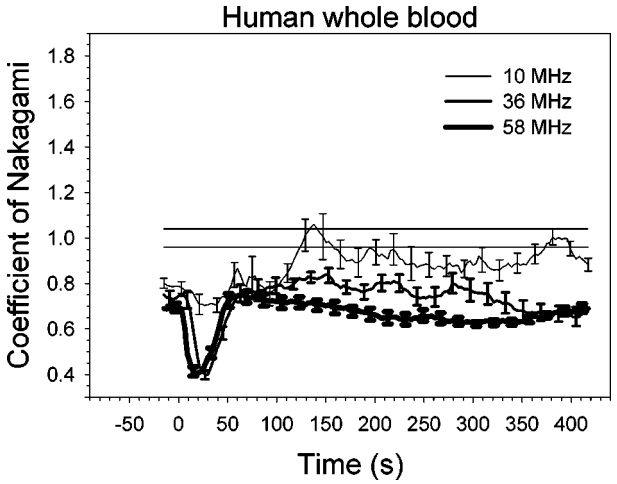

FIG. 8. Coefficient of Nakagami ($\hat{m}$) for human whole blood at a hematocrit of 40%, and a temperature of 37 °C. A time window of 42 s was considered for the computation of $\hat{m}$. The measurements were performed with three transducers at mean frequencies of 10, 36, and 58 MHz. The standard errors are only displayed for selected times to reduce the density of the graphs ($n=15$; three blood samples and five measurements per sample). The horizontal lines correspond to the confidence interval of the estimates $[1\pm G_2(N_s)$, as defined by Eq. (14)].

power changes were investigated. It would have been preferable to measure the absolute backscattering coefficient compensated for the frequency-dependent attenuation, but the experimental setup made this difficult to do.

B. Coefficient of kurtosis

As observed in Fig. 5 for both RBC suspension and whole blood experiments, Gaussian statistics ($\hat{K}_u \approx 3.0$) were obtained at 10 and 36 MHz when the instantaneous rf signals were analyzed. Raising the frequency resulted in an overall significant increase of $\hat{K}_u$ whatever the time instant before or after stopping the flow. For any frequency, the formation of RBC aggregates at $t>0$ did not affect $\hat{K}_u$ when small time windows were considered (the instantaneous analyses of $\hat{K}_u$ were obtained from time windows of 10 ms — i.e., ten records of 1.5 μs at a PRF of 1 kHz). The Gaussian backscattering behavior at 10 and 36 MHz can thus be interpreted from the analysis of Eqs. (3) and (4). For instance, the K-distribution model stipulates that the effective number of scatterers ($M=3/(K_u-3)$) is a function of the actual number of particles (N), and of the lack of uniformity of their cross sections (ν). At a normal hematocrit of 40% (the hematocrit determines the value of N), it can be concluded that the spatial and temporal variations in RBC aggregate sizes (ν) were not sufficient to reduce the value of M for a time window of 10 ms.

A different backscattering behavior was observed for whole blood experiments when longer windows (12–60 s) and the unstationary RBC aggregation process were considered. As seen in Fig. 6 for a time window of 42 s, the non-Gaussian statistics were emphasized at 36 and 58 MHz at the beginning of the kinetics of aggregation. This suggests reductions in the effective number of scatterers ($M=1.25$ for $\hat{K}_u=5.4$) at these frequencies. The lack of uniformity of the backscattering cross sections of scatterers is the mechanism proposed to explain the large increases of $\hat{K}_u$. Similar findings have never been reported in the literature on blood scattering. According to Fig. 6, the 10 MHz probe did not seem to be as sensitive to the presence of a broad range of RBC aggregate sizes within the volume of interest. Because Rayleigh scattering that likely occurs at 10 MHz is theoretically independent of the scatterer shape,[1] this explains why the transitory increases in $\hat{K}_u$ are mainly detected at the highest frequencies.

To our knowledge, Fontaine *et al.*[24] were the only group to study the statistics of the rf signals backscattered by blood. However, their study was based on nonaggregating RBC experiments. In addition, it can be mentioned that few studies investigated the effect of the ultrasound transmitted frequency on non-Gaussian properties of US backscattered signals. All of them were at frequencies below 7.5 MHz. In a study by Chen *et al.*,[19] tissue phantoms were used to demonstrate the effect of the transducer frequency, ultrasound field, and density of scatterers on non-Rayleigh characteristics of the envelope. Deviation from the Rayleigh distribution (reduction of K_u) was observed when the frequency was increased from 3.5 to 5 MHz. These results were explained by the larger ultrasound beam of the 3.5 MHz transducer (the beam incorporated more scatterers). In the present study, the beam profiles were different between the 10, 36, and 58 MHz transducers (the larger beam was at 10 MHz and the smaller one was at 58 MHz; the length of the range cell within the tube was kept close to constant for all transducers). The larger beam may be considered as a confounding factor that could have contributed to the overall tendency toward an increase of $\hat{K}_u$ as a function of frequency. However, the likelihood that this happened is small, considering the large number of RBCs present in the sample volume (at a hematocrit of 40%). Futhermore, it is important to emphasize that changes in the beam width cannot explain the time variations of $\hat{K}_u$ observed in Fig. 6 for a given transducer since the beam characteristics did not change over time.

C. Coefficient of Nakagami

As shown in Figs. 7 and 8, the information conveyed by the coefficient of Nakagami is very similar to that provided by the coefficient of kurtosis. The inverse relation or correlation between both parameters can be appreciated by comparing Eqs. (1) and (6). As introduced earlier, the literature suggests a quasiperiodic half-wavelength spacing of particles for m greater than one, whereas structures showing some level of organization should give values of m between $\frac{1}{2}$ and one.[28] The following explanation is suggested for the results of Figs. 7 and 8. At 10 MHz, since the wavelength is approximately 154 μm, the periodic spacing of RBCs or RBC aggregates may not correspond to half or a larger fraction of the wavelength. Consequently, $\hat{m}$ was close to one, suggesting randomly located particles when *viewed* at such a relatively low spatial resolution. Surprisingly, for a temporal window of 10 ms, $\hat{m}$ reached values close to 1.4 during the kinetics of aggregation (Fig. 7, right panel). Since we observed a lower signal-to-noise ratio at 10 MHz than at the other frequencies, this may reflect a lack of statistical robustness of the Nakagami estimates for the small window of 10 ms. Less variances in the estimates of m were obtained for a window of 42 s (see Fig. 8).

When the frequency was increased to 36 and 58 MHz, the same spacing in the spatial organization of RBCs or RBC aggregates started to be on the order of a fraction of the wavelength, as suggested by the $\hat{m}$ values between $\frac{1}{2}$ and one, for both time windows of 10 ms and 42 s. Interestingly, as shown in Fig. 8, the rapid growth in RBC aggregate sizes between 10 and 25 s following flow stoppage momentarily reduced the Nakagami coefficient at the higher frequencies, which suggest some additional level of spatial organization. It is important to point out here that a thorough analysis of the phase of the rf signals would be required to confirm the existence of spatial coherence among scatterers at a fraction of the wavelength, as suggested in Ref. 46. To our knowledge, the effect of frequencies between 10 and 58 MHz on the Nakagami coefficient has never been addressed. It may be worth mentioning that the values of $\hat{m}<\frac{1}{2}$ observed in Fig. 8 are probably not artifactual. The theoretical lower limit of $\frac{1}{2}$ can be violated for specific conditions (such as a small number of scatterers in the volume of interest), as shown

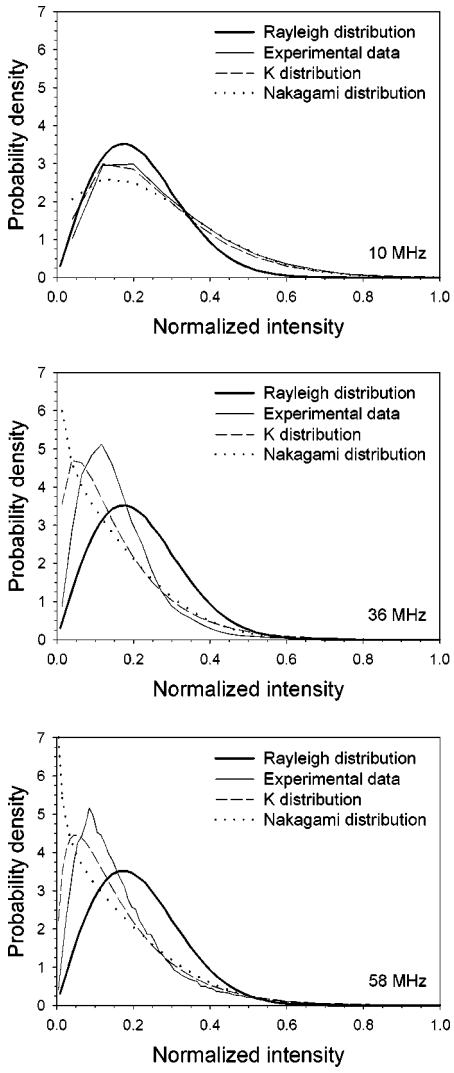

FIG. 9. Normalized probability density distributions of the envelope $A(t)$ of the rf signals backscattered by whole blood for a time window of 42 s, at the peak of $\hat{K}_u$ in Fig. 6 and minimum of $\hat{m}$ in Fig. 8. The data were collected for three transducers at mean frequencies of 10, 36, and 58 MHz. Each panel gives the experimental PDF and those computed from Eq. (2) (K model) and Eq. (5) (Nakagami model). The values of $\hat{K}_u$ (K model) were 3.91, 5.40, and 5.44, and $\hat{m}$ (Nakagami model) were 0.65, 0.39, and 0.38 at 10, 36, and 58 MHz, respectively.

earlier.[28] Finally, one may be cautious with the physical interpretation of $\hat{K}_u$ and $\hat{m}$, because of the inverse correlation between both parameters and the fact that the literature interprets them differently (K_u is affected by the nonuniformity in scattering crosssections, whereas m reflects periodic organization among scatterers; both parameters are influenced by the number of particles in the scattering volume).

D. Validity of the *K* and Nakagami probability density distributions

The validity of the K and Nakagami PDF [Eqs. (2) and (5)] to describe the histogram of $A(t)$ was tested on the data available. For all results in Figs. 5–8 where $\hat{K}_u \approx 3.0$ and $\hat{m} \approx 1.0$, the experimental histogram could adequately be modeled with either the K, Nakagami, or Rayleigh PDF. However, for non-Rayleigh conditions, discrepancies were observed between the experimental histograms and those modeled with Eqs. (2) and (5). For example, Fig. 9 shows probability density distributions of $A(t)$ for whole blood experiments performed with a time window of 42 s, at 10–25 s following flow stoppage (the data corresponding to the maximum of $\hat{K}_u$ in Fig. 6 and minimum of $\hat{m}$ in Fig. 8 were used for this example). At 10 MHz, the K PDF adequately described the experimental histogram of $A(t)$. As the frequency was raised to 36 and 58 MHz, neither the K nor the Nakagami distributions adequately fit the experimental results. This suggest that the physical conclusions extrapolated from these models [effective number density of scatterers, parameter M of Eq. (4); and orderliness in the spatial arrangement of scatterers, Eq. (5)] may not be valid for some of the experimental conditions considered here.

V. CONCLUSION

Experimental measurements of backscattered power changes from human RBC suspensions and whole blood were presented. The most significant power variations were attributed to the phenomenon of RBC aggregation. The backscatter enhancement due to aggregation was shown to decrease with frequency, which agree with recent simulation models.[29,43] It appeared that the time response to rapid changes in scatterer sizes, from individual cells to aggregates of a few RBCs, increased by raising the frequency of the US transducer. Among the three tested frequencies, the best compromise between the echogenicity enhancement and time response was obtained at 36 MHz.

The statistics of the backscattered signals also was investigated by computing the coefficients of kurtosis of the rf signal and the Nakagami parameter on the signal envelope. By computing the statistics over short signal segments (10 ms), Gaussian distributions were obtained at 10 and 36 MHz for both RBC suspension and whole blood experiments ($\hat{K}_u \approx 3.0$ and $\hat{m} \approx 1.0$). Increasing the frequency to 58 MHz modified the statistical nature of the rf backscattered signal to non-Gaussian distributions. By using time windows between 12 and 60 s (only the results for a window of 42 s were presented), a significant non-Gaussian behavior, highly emphasized at the beginning of the kinetics of aggregation, was observed at 36 and 58 MHz. Although attributed to the nonuniformity in backscattering cross sections or to some orderliness in the spatial arrangement of scatterers, it is clear from the results of the current study that the mechanisms of the non-Gaussian backscattering behavior at high frequency may deserve more attention. It was also shown that the K and Nakagami statistical distributions do not always adequately describe the ultrasound signals backscattered by normal human whole blood.

ACKNOWLEDGMENTS

The authors acknowledge Dr. Raymond Beaulieu of the Department of Hematology at the University of Montreal Hospital for providing the human blood samples. This work was supported by operating grants from the Institutes of Health Research of Canada (Grant No. MOP-36467) and the Heart and Stroke Foundation of Quebec, and by an equip-

ment grant from the Foundation of the University of Montreal Hospital (ultrasound biomicroscope). The salary of Dr. Guy Cloutier is partially supported by a National Scientist award of the Fonds de la Recherche en Santé du Québec.

[1] K. K. Shung and G. A. Thieme, *Ultrasonic Scattering in Biological Tissues*, edited by K. K. Shung and G. A. Thieme (CRC, Boca Raton, 1993).
[2] G. Cloutier and Z. Qin, ''Ultrasound backscattering from non-aggregating and aggregating erythrocytes-A review,'' Biorheology **34**, 443–470 (1997).
[3] F. S. Foster, H. Obara, T. Bloomfield, L. K. Ryan, and G. R. Lockwood, ''Ultrasound backscatter from blood in the 30 to 70 MHz frequency range,'' IEEE Ultrasonics Symposium Proceedings, 1994, Vol. 3, Nov. 1–4, Cannes, France, pp. 1599–1602.
[4] A. van Lewenhoek, ''Concerning the circulation and stagnation of the blood in tadpoles,'' Philos. Trans. R. Soc. London **22**, 447 (1702).
[5] R. Fahraeus, ''The suspension stability of the blood,'' Physiol. Rev. **IX**, 241–275 (1929).
[6] H. J. Meiselman, ''Red blood cell role in RBC aggregation: 1963–1993 and beyond,'' Clin. Hemorheol. **13**, 575–592 (1993).
[7] M. H. Knisely, E. H. Bloch, T. S. Eliot, and L. Warner, ''Sludged blood,'' Science **106**, 431–440 (1947).
[8] S. Chien, ''Blood viscosity: Influence of erythrocyte aggregation,'' Science **157**, 829–831 (1967).
[9] A. Chabanel, M. H. Horellou, J. Conard, and M. M. Samama, ''Red blood cell aggregability in patients with a history of leg vein thrombosis: influence of post-thrombotic treatment,'' Br. J. Haematol. **88**, 174–179 (1994).
[10] M. Cabel, H. J. Meiselman, A. S. Popel, and P. C. Johnson, ''Contribution of red blood cell aggregation to venous vascular resistance in skeletal muscle,'' Am. J. Physiol. **272**, H1020–H1032 (1997).
[11] M. J. Pearson and H. H. Lipowsky, ''Influence of erythrocyte aggregation on leukocyte margination in postcapillary venules of rat mesentery,'' Am. J. Physiol. **279**, H1460–H1471 (2000).
[12] J. J. Bishop, P. R. Nance, A. S. Popel, M. Intaglietta, and P. C. Johnson, ''Effect of erythrocyte aggregation on velocity profiles in venules,'' Am. J. Physiol. **280**, H222–H236 (2001).
[13] N. Maeda, ''Erythrocyte rheology in microcirculation,'' Jpn. J. Physiol. **46**, 1–14 (1996).
[14] C. Dupuy-Fons, J. F. Brun, F. Pellerin, J. C. Laborde, L. Bardet, A. Orsetti, and C. Janbon, ''Relationships between blood rheology and transcutaneous oxygen pressure in peripheral occlusive arterial disease,'' Clin. Hemorheol. **15**, 191–199 (1995).
[15] G. Cloutier, X. Weng, G. O. Roederer, L. Allard, F. Tardif, and R. Beaulieu, ''Differences in the erythrocyte aggregation level between veins and arteries of normolipidemic and hyperlipidemic individuals,'' Ultrasound Med. Biol. **23**, 1383–1393 (1997).
[16] R. Kuc, ''Ultrasonic tissue characterization using kurtosis,'' IEEE Trans. Ultrason. Ferroelectr. Freq. Control **UFFC-33**, 273–279 (1986).
[17] M. Evans, N. Hastings, and B. Peacock, Statistical Distributions, 3rd ed. (Wiley, New York, 2000).
[18] L. Weng, J. M. Reid, P. M. Shankar, and K. Soetanto, ''Ultrasound speckle analysis based on the *K* distribution,'' J. Acoust. Soc. Am. **89**, 2992–2995 (1991).
[19] J. F. Chen, J. A. Zagzebski, and E. L. Madsen, ''Non-Gaussian versus non-Rayleigh statistical properties of ultrasound echo signals,'' IEEE Trans. Ultrason. Ferroelectr. Freq. Control **41**, 435–441 (1994).
[20] P. M. Shankar, J. M. Reid, H. Ortega, C. W. Piccoli, and B. B. Goldberg, ''Use of non-Rayleigh statistics for the identification of tumors in ultrasonic B-scans of the breast,'' IEEE Trans. Med. Imaging **12**, 687–692 (1993).
[21] V. M. Narayanan, P. M. Shankar, and J. M. Reid, ''Non-Rayleigh statistics of ultrasonic backscattered signals,'' IEEE Trans. Ultrason. Ferroelectr. Freq. Control **41**, 845–852 (1994).
[22] R. C. Molthen, P. M. Shankar, J. M. Reid, F. Forsberg, E. J. Halpern, C. W. Piccoli, and B. B. Goldberg, ''Comparisons of the Rayleigh and *k*-distribution models using *in vivo* breast and liver tissue,'' Ultrasound Med. Biol. **24**, 93–100 (1998).
[23] P. M. Shankar, R. Molthen, V. M. Narayanan, J. M. Reid, V. Genis, F. Forsberg, C. W. Piccoli, A. E. Lindenmayer, and B. B. Goldberg, ''Studies of the use of non-Raleigh statistics for ultrasonic tissue characterization,'' Ultrasound Med. Biol. **22**, 873–882 (1996).
[24] I. Fontaine, G. Cloutier, and L. Allard, ''Non-Gaussian statistical property of the ultrasonic Doppler signal downstream of a severe stenosis,'' Ultrasound Med. Biol. **23**, 41–45 (1997).
[25] R. F. Wagner, M. F. Insana, and D. G. Brown, ''Unified approach to the detection and classification of speckle texture in diagnostic ultrasound,'' Opt. Eng. (Bellingham) **25**, 738–742 (1986).
[26] V. Dutt and J. F. Greenleaf, ''Ultrasound echo envelope analysis using a homodyned *K* distribution signal model,'' Ultrasonic Imaging **16**, 265–287 (1994).
[27] R. B. Cramblitt and K. J. Parker, ''Generation of Non-Rayleigh speckle distributions using marked regularity models,'' IEEE Trans. Ultrason. Ferroelectr. Freq. Control **46**, 867–874 (1999).
[28] P. M. Shankar, ''A general statistical model for ultrasonic backscattering from tissues,'' IEEE Trans. Ultrason. Ferroelectr. Freq. Control **47**, 727–736 (2000).
[29] D. Savéry and G. Cloutier, ''A point process approach to assess the frequency dependence of ultrasound backscattering by aggregating red blood cells,'' J. Acoust. Soc. Am. **110**, 3252–3262 (2001).
[30] I. Fontaine, D. Savéry, and G. Cloutier, ''Simulation of ultrasound backscattering by red cell aggregates: Effect of shear rate and anisotropy,'' Biophys. J. **82**, 1696–1710 (2002).
[31] Z. Qin, L. G. Durand, L. Allard, and G. Cloutier, ''Effects of a sudden flow reduction on red blood cell rouleau formation and orientation using rf backscattered power,'' Ultrasound Med. Biol. **24**, 503–511 (1998).
[32] D. W. Rickey, P. A. Picot, D. A. Christopher, and A. Fenster, ''A wall-less vessel phantom for Doppler ultrasound studies,'' Ultrasound Med. Biol. **21**, 1163–1176 (1995).
[33] L. L. Houbouyan, M. Delamaire, A. Beauchet, M. Gentil, G. Cauchois, A. Taccoen, J. P. Yvert, N. Montredon, M. F. Roudaut, S. Zhao, A. Goguel, G. Potron, M. Boisseau, and J. F. Stoltz, ''Multicenter study of an erythroaggregometer: quality control and standardization,'' Clin. Hemorheol. Microcirc. **17**, 299–306 (1997).
[34] P. J. Carreau, D. C. R. De Kee, and R. P. Chhabra, *Rheology of Polymeric Systems: Principles and Applications* (Hanser, Munich, 1997).
[35] X. Weng, G. Cloutier, P. Pibarot, and L. G. Durand, ''Comparison and simulation of different levels of erythrocyte aggregation with pig, horse, sheep, calf, and normal human blood,'' Biorheology **33**, 365–377 (1996).
[36] X. Weng, G. Cloutier, R. Beaulieu, and G. O. Roederer, ''Influence of acute-phase proteins on erythrocyte aggregation,'' Am. J. Physiol. **271**, H2346–H2352 (1996).
[37] K. K. Shung, Y. W. Yuan, D. Y. Fei, and J. M. Tarbell, ''Effect of flow disturbance on ultrasonic backscatter from blood,'' J. Acoust. Soc. Am. **75**, 1265–1272 (1984).
[38] K. K. Shung, G. Cloutier, and C. C. Lim, ''The effects of hematocrit, shear rate, and turbulence on ultrasonic Doppler spectrum from blood,'' IEEE Trans. Biomed. Eng. **39**, 462–469 (1992).
[39] G. R. Lockwood, L. K. Ryan, J. W. Hunt, and F. S. Foster, ''Measurement of the ultrasonic properties of vascular tissues and blood from 35–65 MHz,'' Ultrasound Med. Biol. **17**, 653–666 (1991).
[40] M. S. Van Der Heiden, M. G. M. De Kroon, N. Bom, and C. Borst, ''Ultrasound backscatter at 30 MHz from human blood: influence of rouleau size affected by blood modification and shear rate,'' Ultrasound Med. Biol. **21**, 817–826 (1995).
[41] V. Rouffiac, P. Péronneau, A. Hadengue, A. Barbet, P. Delouche, P. Dantan, N. Lassau, and J. Levenson, ''A new ultrasound principle for characterizing erythrocyte aggregation - In vitro reproducibility and validation,'' Invest. Radiol. **37**, 413–420 (2002).
[42] S. Y. Kim, I. F. Miller, B. Sigel, P. M. Consigny, and J. Justin, ''Ultrasonic evaluation of erythrocyte aggregation dynamics,'' Biorheology **26**, 723–736 (1989).
[43] I. Fontaine, and G. Cloutier, ''Modeling the frequency dependence (5–120 MHz) of ultrasound backscattering by red cell aggregates in shear flow at a normal hematocrit,'' J. Acoust. Soc. Am. **113**, 2893–2900 (2003).
[44] G. Cloutier and K. K. Shung, ''Study of red cell aggregation in pulsatile flow from ultrasonic Doppler power measurements,'' Biorheology **30**, 443–461 (1993).
[45] M. G. M. De Kroon, C. J. Slager, W. J. Gussenhoven, P. W. Serruys, J. R. T. C. Roelandt, and N. Bom, ''Cyclic changes of blood echogenicity in high-frequency ultrasound,'' Ultrasound Med. Biol. **17**, 723–728 (1991).
[46] V. M. Narayanan, R. Molthen, P. M. Shankar, L. Vergara, and J. M. Reid, ''Studies on ultrasonic scattering from quasi-periodic structures,'' IEEE Trans. Ultrason. Ferroelectr. Freq. Control **44**, 114–124 (1997).